Conformational Analysis of an α3β1 Integrin-Binding Peptide from Thrombospondin-1: Implications for Antiangiogenic Drug Design[1]

Julien Furrer,[†] Burkhard Luy,[†] Venkatesha Basrur,[§,⊥] David D. Roberts,[‡,*] and Joseph J. Barchi, Jr.[∥,*]

Institut für Organische Chemie and Biochemie II, Technische Universität Muenchen, Garching, Germany, Laboratory of Pathology and Laboratory of Cell Biology, Center for Cancer Research, National Cancer Institute, National Institutes of Health, Bethesda, Maryland 20892, and Laboratory of Medicinal Chemistry, Center for Cancer Research, National Cancer Institute at Frederick, National Institutes of Health, Frederick, Maryland 21702

Received July 15, 2006

The integrin α3β1 plays important roles in development, angiogenesis, and the pathogenesis of cancer, suggesting potential therapeutic uses for antagonists of this receptor. Recently, an α3β1 integrin-binding site was mapped to residues 190−201 (FQGVLQNVRFVF) of the N-terminal domain of the secreted protein thrombospondin-1 (TSP1). This sequence displays diverse biological activities in vitro and inhibits angiogenesis in vivo. Herein we describe the NMR solution conformation of this segment in both water and dodecylphosphocholine micelles. While essentially unstructured in water, a more well-defined conformation is populated in micelles, particularly in the C-terminal half of the peptide and correlated with increased biological activity of the micellar peptide. The data suggested that the residues that are critical for biological activity are contained in a structurally well-defined segment of the peptide. These data support the role of the NVR motif as a required element of full-length TSP1 for specific molecular recognition by the α3β1 integrin.

Introduction

Integrins play crucial roles in mediating cell−matrix interactions and as signaling molecules to regulate cell survival, growth, motility, and differentiated functions[1,2] Each of the 24 known integrins binds specifically to one or more extracellular matrix ligands, usually in a divalent cation-dependent manner.[3] In some cases, specific linear amino acid motifs have been defined that are required for this recognition, and crystal structures of both integrins and their ligands have validated their roles in integrin recognition.[4,5] The first such motif identified is the RGD sequence recognized by α5β1 and αvβ3 integrins.[6] In fibronectin, this motif exists in an exposed loop in the tenth type 3 repeat,[7] and cyclic peptides that stabilize this conformation exhibit enhanced inhibitory activities[3,8]

Not all integrin ligands contain an RGD motif, however, and some integrin−ligand interactions are not inhibited by RGD peptides. Additional recognition motifs have been identified, many of which have a conserved Asp or Glu residue.[9−11] For some integrins, inhibitory peptides have been identified that lack an acidic residue. This is the case for α3β1 integrin, for which inhibitory peptides have been identified from its ligands, the laminins and thrombospondin-1 (TSP1[a]).[1,12,13] The active peptide GD6 was derived from a G module in the C-terminal region of the laminin A chain.[12] The binding site for α3β1 in TSP1 was mapped to residues 175−242 in the N-terminal globular domain (TSPN-1). A 12-mer peptide from this region (residues 190−201) was shown to be a potent inhibitor of cell adhesion on TSP1 or murine laminin-1 and exhibited α3β1-dependent adhesive and proliferative activities when adsorbed on plastic.[13−15] The motif NVR in this peptide was shown to be essential for activity, and this sequence is conserved in all known mammalian TSP1 sequences as well as in TSP1 from *Xenopus laevis*.[13]

Recently, a crystal structure of the TSPN-1 domain which includes residues 190−201 has been solved by the Lawler group.[16] This domain is evolutionarily related to the α3β1-binding G-modules of laminins and to the pentraxin family.[17] Residues 190−201 were shown to comprise the final strand (β14) of a β-sheet that runs along the "back" face of TSPN-1, qualitatively confirming the results of modeling of a TSP1 N-module structure[18] based on these known pentraxin folds.[13] The crystal structure also confirms that most of the hydrophobic residues in the TSP1 peptide lie at the interface between opposing β-sheets and are hidden from solvent, while N196 and R198 of the critical NVR motif are the only solvent-exposed residues capable of binding to α3β1 integrins. Given these data, the stage is now set for the structure-based design of peptidomimetics of these biologically important motifs.

In this report, we describe the three-dimensional solution structure of the 12-residue TSPN-1 peptide that comprises residues 190−201 (FQGVLQNVRFVF) dissolved in H_2O and in DPC-Micelles. We employed a lipid environment for the structural analysis based on the following: (1) This sequence in TSP1 was predicted (and is now shown)[16] to exist in a protein fold wherein opposite faces would be in aqueous and nonpolar environments, (2) the solubility of the 12-mer peptide (heretofore referred to as peptide $TSP1_{678}$ according to the original reference[13]) was far superior in micelles, and (3) the biological activity of $TSP1_{678}$ was enhanced in the presence of various lipids (see Results). While the structure in H_2O solution shows more or less an extended peptide chain, the C-terminal 7 residues

* Corresponding authors. D.D.R., Chief, Biochemical Pathology Section, Bldg. 10, Rm. 2A33, 10 Center Dr. MSC1500, Bethesda, MD 20892. Phone: (301) 496-6264. Fax: (301) 402-0043. E-mail: droberts@helix.nih.gov. J.J.B., National Cancer Institute, Frederick, 376 Boyles St., PO Box B, Bldg. 376, Rm. 209, Frederick, MD 21702. Phone: (301) 846-5905. Fax: (301) 846-6033. E-mail: barchi@helix.nih.gov.

† Technische Universität Muenchen.

‡ Laboratory of Pathology, NIH, Bethesda.

§ Laboratory of Cell Biology, NIH, Bethesda.

∥ Laboratory of Medicinal Chemistry, NIH, Frederick.

⊥ Present address: Department of Bioinformatics and Proteomics/Genomics, University of Toledo, Toledo, OH 43614-5806.

[a] Abbreviations used: TSP1, thrombospondin-1; DPPC, dipalmitoyl phosphatidylcholine; DPC, dodecylphosphocholine; MOCCA, MOdified phase Cycled CArr-Purcell-type; ICAM-1, intercellular adhesion molecule-1.

10.1021/jm060833l CCC: $33.50
Published on Web 09/22/2006

of $TSP1_{678}$ are well structured when bound to DPC micelles. The data suggest that the structure of $TSP1_{678}$ in DPC micelles reproduces the overall disposition of the NVR motif in the full TSPN-1 domain. This information should provide further insight into the shape of the binding surface of the essential core NVR element in the context of a small peptide as a prelude to future drug design.

Materials and Methods

The 1−12 numbering system was used throughout to describe the TSP_{678} peptide, and these residues in turn correspond to residue numbers 190−201 in the protein structure.[16] Dipalmitoyl phosphatidylcholine (DPPC), dimyristoyl phosphatidylcholine, cholesterol, dipalmitoyl phosphatidylethanolamine, dipalmitoyl phosphatidylglycerol, *p*-nitrophenyl-*β*-*N*-acetylglucosamine, and bovine serum albumin were obtained from Sigma. Dodecylphosphocholine (DPC)-d_{38} was purchased from Avanti Polar Lipids (Alabaster, AL). All peptides studied herein (cf. Table 3) were synthesized as described previously.[13] MDA-MB-435 breast carcinoma cells and the hybridoma secreting β1 integrin antibody TS2/16 were obtained from the American Type Culture Collection (Manassas, VA).

CD Spectroscopy. Far UV circular dichroism measurements were made at 25 °C using a Jasco J715 spectropolarimeter. All solvents were extensively degassed, and spectra were recorded using a bandwidth of 2 nm with a scan speed of 20 nm/min in a 0.2 cm path length cuvette. Each sample (20 μM) was scanned 10 times, and average ellipticities between 205 and 250 nm, after subtracting the buffer reading, were used to calculate the mean residue ellipticity ($[\theta]_{MRW}$) using the equation

$$[\theta]_{MRW} = (\theta \times M_{MRW})/10 \times C \times l \quad (1)$$

where θ is the observed ellipticity, M_{MRW} is the mean residue M_r (110.4 amu), C is the concentration of peptide in mg/mL, and l is path length in centimeters.

NMR Spectroscopy. Initially, samples were prepared by dissolving ca. 0.8 mg of the peptide in 330 μL of $^1H_2O/^2H_2O$ (9:1), resulting in a $TSP1_{678}$ concentration of approximately 1.8 mM. At this concentration, the solution was highly viscous resulting in very broad ^{1}H NMR signals. The sample was diluted in several steps until spectra showed a consistent line width of approximately 4−5 Hz and no changes in chemical shifts. This final concentration of $TSP1_{678}$ that was employed for structure determination was approximately 0.2 mM.

For the study of TSP-1 in [^{2}H]DPC micelles, a 210 mM DPC solution was prepared by first dissolving 28 mg of [^{2}H]DPC in 330 μL of $^1H_2O/^2H_2O$ (9:1) and then adding the peptide. Initially, ca. 2 mg of $TSP1_{678}$ was added to the solution and a set of NMR experiments acquired. At this concentration the solution again appeared to be very viscous, and several sets of resonances could be identified in the NMR spectra with very broad line widths, most likely originating from different aggregated states of the peptide or from multiple conformations resulting from partial dissolution in lipid. The sample was then diluted twice with a 210 mM DPC solution to a final peptide concentration of approximately 0.3 mM. Under these conditions, there remained several minor but observable sets of resonances in the spectra. However, a distinctly dominant set of resonances was present at this concentration. Since we must assume that the predominance of this set of resonances will be increased upon dilution and whereas further dilution would have made the acquisition of two-dimensional spectra with reasonable quality impossible, we decided to carry out the structure determination of this major conformation of $TSP1_{678}$ in this mixture.

All NMR experiments were performed at 300 K on Bruker (Karlsruhe, Germany) AVANCE DRX spectrometers operating at nominal ^{1}H frequencies of 600, 750, and 900 MHz, equipped with 5 mm ^{1}H inverse triple resonance cryoprobes (600 and 900 MHz) with pulsed field gradients along the *z* axis and with a 5 mm ^{1}H inverse quadruple resonance probe head with triple axes pulsed field gradients (750 MHz). Two-dimensional (2D) NMR spectra were acquired in the phase sensitive mode using either the States-TPPI[19] or the echo-antiecho method,[20,21] in the indirectly detected dimension. Water suppression was achieved in all cases by using the W5 sequence[22] and the DPFGSE technique.[23] Additional water presaturation and bipolar gradients within both the t_1 evolution time and the NOESY mixing time were also used to avoid radiation damping. The spectral width used was 14.018 ppm for ^{1}H for all experiments. The NMR data were processed using XWin-NMR software, version 3.5 (Bruker), and analyzed using the Sparky software package (vs 3.106).[24] Zero-filling to 4096 × 2048 points, 60° shifted sine-bell apodization (t_1 and t_2). and baseline corrections in both dimensions were performed prior to Fourier transformations.

Experiments and Resonance Assignment for $TSP1_{678}$ in $H_2O/^2H_2O$ (9:1). ^{1}H resonance assignments of individual spin systems were obtained using a gradient-selected homonuclear TOCSY experiment at 600 MHz with a mixing time of 70 ms employing the DIPSI-2 multiple pulse sequence[25,26,27] for generation of the spin lock segment. The data size was 512 × 2048 complex points collected in 64 scans per increment. For the identification of through space correlations and sequential assignments, a 2D Compensated ROESY spectrum[28,29] with a mixing time of 200 ms (data size 512 × 2048 complex points, spin lock = 5 kHz, 256 scans/ increment) was also recorded at 600 MHz. Chemical shifts were indirectly referenced via Ξ ratios.[30]

Experiments and Resonance Assignment for $TSP1_{678}$ in [$^2H_{38}$]-DPC in $H_2O/^2H_2O$ (9:1). For ^{1}H intraresidual resonance assignments several gradient-selected homonuclear TOCSY experiment (data size 768 × 2048 complex points, 128 scans) with typical mixing times of 70 ms were recorded at 750 MHz field strength. Best results were obtained using the relaxation-optimized MOCCA-XY16 multiple pulse sequence[31] for the TOCSY mixing period. However, the quality of the spectra was poor in all cases with partially smeared cross-peaks due to the presence of a number of conformations and/or line-broadening due to exchange phenomena. For the identification of through space correlations, a NOESY spectrum (mixing time of 80 ms, data size 512 × 4096 complex points, 256 scans) was recorded at 900 MHz. This spectrum was of significantly higher quality than the TOCSY spectra recorded, with the intensity of cross-peaks of the major conformation on average about 10 times more intense than those resulting from other conformations. Therefore, the amino acid and sequential assignments in practice were obtained by starting from NOESY cross-peaks followed by analysis of the MOCCA-XY16 TOCSY spectrum to confirm the assignment. Chemical shifts were indirectly referenced via the Ξ ratios.[30] ^{1}H−^{13}C HSQC spectra were acquired for the sample, but even after 24 h experiment time at 750 MHz the quality of the spectra remained poor. The spectra were used in some cases as support for the ^{1}H-assignment, but a general ^{13}C-assignment was not attempted.

Structure Calculations. Analysis of 2D NOESY and ROESY spectra provided the distance constraints for protons, based on the corresponding cross-peak intensities. For $TSP1_{678}$ dissolved in 9:1 $H_2O/^2H_2O$, ROE cross-peak volumes were calibrated against cross-peak intensities between well-separated geminal $F12_{H\beta1}$−$F12_{H\beta2}$ signals, for which the distance has been set to 1.788 Å. Lower and upper distance bounds of 0.5 Å were then added to the derived distances to allow for errors in spectral intensities, and slightly larger errors were added to partially overlapped resonances. The standard ROESY offset correction for the compensated-ROESY experiment[23] was applied prior to the conversion into distances. Lower and upper distance bounds of 0.5 Å and 1.0 Å, respectively, were added to the derived distances to allow for errors in spectral intensities and partially overlapped resonances. Structure calculations were performed with the program X-PLOR,[32] using standard simulated annealing protocols with floating chirality developed for peptides and proteins. In the final run, a set of 100 structures was computed for the peptide, and the 20 lowest energy structures were used for interpretation.

Due to the significant molecular weight of the complex, $TSP1_{678}$ in DPC micelles was treated like a medium-sized protein. NOE cross-peak intensities again were calibrated against cross-peak

intensities between the well-separated geminal $F12_{H\beta1}-F12_{H\beta2}$ signals. Cross-peaks were thus divided into classes with respect to their intensities, which resulted in distance restraint classes of 2.5, 3.0, 4.0, and 5.0 Å, respectively. Lower and upper distance bounds of 0.5 Å and 1.0 Å, respectively, were added to the derived distance classes to allow for errors in spectral intensities and partially overlapped resonances. The structure of $TSP1_{678}$ in DPC micelles was calculated in the same way as the peptide in water using X-PLOR[32] with standard simulated annealing protocols with floating chirality (a prochiral assignment of side chain protons could not reliably be achieved with the available NMR data). Again, a final set of 100 structures was calculated and the 20 structures with lowest overall energy were used for interpretation.

Cell Adhesion Assays. Cell adhesion to peptides immobilized in 96-well microtiter plates was determined using a colorimetric assay as previously described.[33] Briefly, peptides were adsorbed onto wells of Nunc Maxisorp plates either by partitioning from aqueous phosphate-buffered saline, pH 7.3, or from 50 μL of 50% aqueous methanol containing the indicated concentrations of peptide and 50 ng of the indicated phospholipids or 30 ng of cholesterol. The methanol/water solutions were incubated for 1 h uncovered in air to evaporate the methanol and then covered and incubated overnight at 4°. The wells were aspirated, blocked with 1% bovine serum albumin, and incubated with 7000 MDA-MB-435 cells/well in RMPI 1640 medium containing 0.1% bovine serum albumin for 1 h in a humidified CO_2 incubator. After being washed to remove nonattached cells, adherent cells were quantified by an assay of cellular hexosaminidase activity using *p*-nitrophenyl-*β*-*N*-acetyl-glucosamine as substrate. All assays were performed in triplicate, and results are presented as mean ± SD.

Results

Active Analogues of $TSP1_{678}$ Have Similar Secondary Structures. Two peptides recognized by $\alpha3\beta1$ integrin, the native TSP1 sequence FQGVLQNVRFVF ($TSP1_{678}$, $IC_{50} = 3.5$ μM) and FQGVLQNV**K**FVF ($TSP1_{702}$, $IC_{50} = 6$ μM), showed similar CD spectra in water. Both displayed negative peaks at 223−227 and 212−216 nm (Figure 1A) followed by a characteristic split in the Cotton effect to positive ellipticity near end absorption (<210 nm). In contrast, the inactive analogues FQGVLQNV**A**FVF ($TSP1_{690}$), FQGVLQNV**Q**FVF ($TSP1_{703}$), and FQGVLQN**A**RFVF ($TSP1_{691;}$ IC_{50} values > 300 μM for $TSP1_{690}$ and $TSP1_{691}$; > 100 μM for $TSP1_{703}$) consistently lacked these spectral signatures (Figure 1A and data not shown). FQGVLQ**A**VRFVF ($TSP1_{686}$) has minimal inhibitory activity in solution ($IC_{50} \sim 300$ μM) but supports $\alpha3\beta1$-mediated cell adhesion and neurite outgrowth at 40−60% that of $TSP1_{678}$ when immobilized on polystyrene.[13,14] This weakly active analogue gave a similar absorption pattern as $TSP1_{678}$ but at diminished signal intensity (Figure 1A). Thus, these CD spectral features correlated with the $\alpha3\beta1$ integrin binding activities of the peptides. Normalized CD spectra for $TSP1_{678}$ in water were independent of peptide concentration over the range of 1 to 100 μM, suggesting that no aggregation occurs at these molarities (data not shown).

The native $TSP1_{678}$ peptide gave similar CD spectra in both water and PBS (pH 7.4, Figure 1B). The inactive peptide $TSP1_{691}$ also lacked structure in PBS. Although previous functional characterization of these peptides was conducted in isotonic buffers,[13−15] these data indicate that the active TSP1 peptides retain a similar conformation in water. Therefore, structural studies conducted in aqueous solution should reflect the active conformation of this peptide.

NMR Description of the Structure of $TSP1_{678}$ in H_2O. The $TSP1_{678}$ peptide was synthesized as described in Materials and Methods and subsequently used for two-dimensional ^1H NMR experiments. The solubility of $TSP1_{678}$ in water was low due to the primarily hydrophobic nature of the sequence. At millimolar concentrations, aggregation of the peptide was observed and the solution was highly viscous. Dilution of samples to a concentration of approximately 0.1−0.2 mM resolved the aggregation problem and gave reproducible results. At this low concentration, however, NMR structural studies proved challenging and could only be successfully achieved using high field spectrometers equipped with cryogenic probeheads. Despite this, several experiments performed at 300 K allowed for nearly complete ^1H resonance assignments (Table 1). The TOCSY and ROESY spectra facilitated assignment of individual spin systems and sequence connectivities, respectively. Difficulties in the assignments arose due to resonance

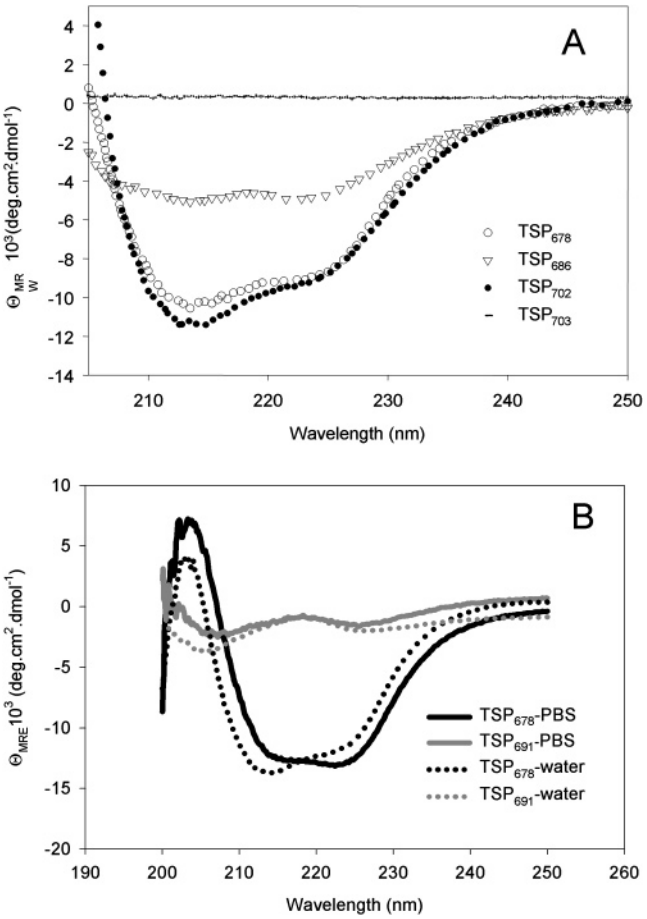

Figure 1. CD spectra of TSP1 peptide analogues. (A) Spectra for peptides 678, 686, 702, 703 (see Table 3) were determined at 20 μM in water. (B) Spectra for 678 and 691 in water vs PBS.

Table 1. ^1H Chemical Shifts of $TSP1_{678}$ in H_2O

	chemical shift (ppm)			
residue	NH	$C^{\alpha}H$	$C^{\beta}H$	others
Phe[1]	8.31	4.17	2.87	n.r.[a]
Gln[2]	8.51	4.28	1.84; 1.5	γCH_2 2.22; δNH_2 7.41
Gly[3]	8.05	3.85	-	-
Val[4]	8.04	4.05	1.97	γCH_3 0.84
Leu[5]	8.31	4.26	1.46	γH 1.53; δCH_3 0.81; 0.75
Gln[6]	8.29	4.21	1.85; 1.97	γCH_2 2.22; δNH_2 7.41
Asn[7]	8.38	4.57	2.64; 2.71	δNH_2 7.49
Val[8]	7.91	3.96	1.93	γCH_3 0.78; 0.73
Arg[9]	8.18	4.18	1.44; 1.57	γCH_2 1.34; δCH_2 3.04; ϵNH 7.03
Phe[10]	8.17	4.52	2.85; 2.93	δH 7.09[b]
Val[11]	7.78	3.96	1.84	γCH_3 0.74
Phe[12]	7.77	4.36	2.87; 3.06	δH 7.4[b]

[a] Not resolved. [b] Missing aromatic proton chemical shifts were not resolved and could not be unambiguously identified.

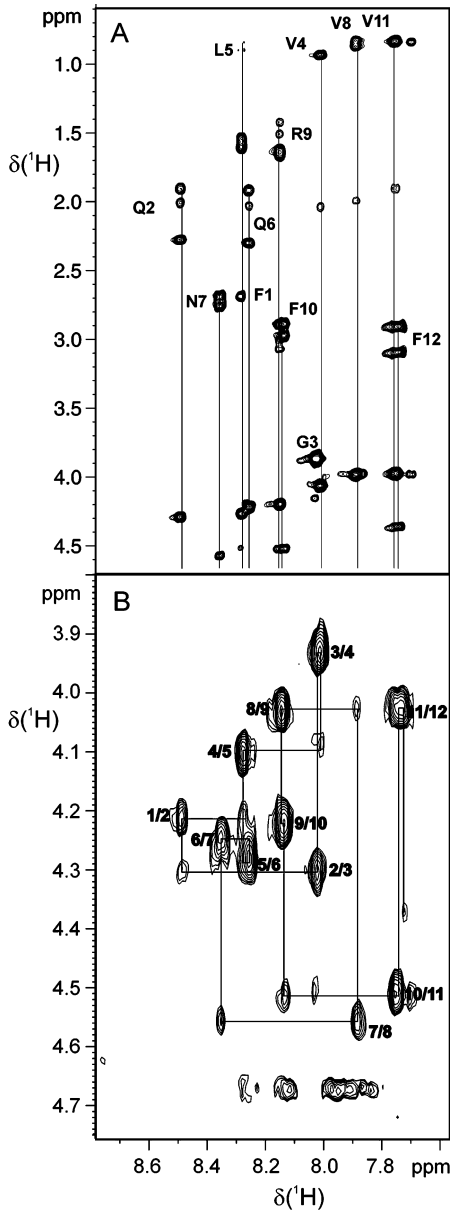

Figure 2. Fingerprint region of the 70 ms TOCSY spectrum (A) and the H_N-H_α region of the 200 ms ROESY spectrum (B) of $TSP1_{678}$ dissolved in 9:1 $^1H_2O/^2H_2O$ (9:1). The individual spin systems are connected with vertical lines and assigned by one-letter amino acid codes in the TOCSY. The sequential walk is demonstrated in the ROESY spectrum with interresidual cross-peaks labeled with the amino acid number.

degeneracy and overlap in the amide resonances as follows: Phe1, Leu5 (8.31 ppm), which also partially overlap with Gln6 (8.29 ppm); Arg9 and Phe10 (8.15 ppm); Val11 and Phe12 (7.77 ppm). Nevertheless, good dispersion of the $H_\alpha-H_N$ and $H_\beta-H_N$ cross-peaks permitted unambiguous assignment of all amino acid spin systems. An expansion of the fingerprint region of the TOCSY spectrum obtained for $TSP1_{678}$ in H_2O is shown in Figure 2A along with the sequential walk analysis in the ROESY spectrum in which individual amino acid assignments are highlighted (Figure 2B).

Short peptides such as $TSP1_{678}$ usually show a high degree of flexibility in solution with a significant number of conformations in fast exchange. These random-coil structures lack any diagnostic medium and long-range distance restraints, and hence the only measures of preferred conformations in the overall population must be derived from other more qualitative parameters. One of these measures is the analysis of secondary chemical shifts relative to random coil values.[30] For $TSP1_{678}$ in H_2O, the chemical shifts of the H_α and H_N resonances of residues Gln6 to Phe12 are shifted slightly upfield compared to random coil, which may be interpreted as a propensity to form some defined structural element in fast exchange in solution. The distance restraints derived from the ROESY experiment only lead to intraresidue and (*i*,*i*+1) interresidue connectivities, and thus structure calculations performed according to the procedures described in Materials and Methods (see Table 2) expectedly resulted in an elongated peptide, essentially devoid of secondary structural elements. $J_{H\alpha--HN}$ coupling constants of ~7 Hz could be measured for almost all residues, which further supported the extended nature of the backbone of the averaged structures of $TSP1_{678}$ in H_2O. The only suggestion that a structured intermediate conformation may be present was seen in the superposition of residues 7−9 in the 20 best calculated structures, where a slight bend is conserved due to a number of (*i*,*i*+1) interresidual distance restraints (cf. Figure 6A). This might be of special interest, since these residues form the necessary motif for the interaction of $TSP1_{678}$ with α3β1 integrins.

Table 2. Structural Statistics of the 12 Best NOE-Derived Structures of $TSP1_{678}$ in H_2O

total no. of distance constraints	60
no. of intraresidue constraints	37
no. of sequential constraints	23
no. of medium to long-range constraints	0
distance violations	
number > 0.5 Å	0
number > 0.2 Å	1.92 ± 0.31 (1.. 3)
RMS deviations from ideal geometry	
covalent bonds (Å)	0.0036 ± 0.0005 (0.003.. 0.004)
covalent angles (Å)	0.5469 ± 0.0221 (0.509.. 0.613)
improper (deg)	0.2766 ± 0.0131 (0.259.. 0.304)
NOE	0.0892 ± 0.0019 (0.066.. 0.107)
energies (kcal/mol)	
overall	52.16 ± 4.16 (38.95.. 58.89)
bond	2.48 ± 0.44 (1.46.. 3.11)
angle	17.13 ± 1.40 (14.77.. 21.44)
improper	1.00 ± 0.07 (0.90.. 1.17)
VDW	9.33 ± 1.90 (4.62.. 12.39)
NOE	22.19 ± 5.17 (11.07.. 30.28)
pairwise RMSD (Å)	
residues 7-9	
backbone	0.60
heavy	2.12

Structure−Activity Relationships of $TSP1_{678}$ Analogues. We previously showed that the arginine residue at position 9 is critical for inhibition of α3β1 integrin-dependent adhesion of breast cancer cells.[13] Inhibitory activities of several additional modifications of the sequence for α3β1-dependent cell adhesion are outlined in Table 3. Replacement of Arg9 with other basic residues retains activity whereas removal of the charge by substitution with a glutamine to retain hydrogen-bonding capacity abrogates the inhibition and suggests a specific ionic interaction of this side chain with the integrin. Two additional one amino acid substitutions proved that either a one methylene extension of the Asn7 to Gln or placing an acidic residue at position 7 maintained (albeit slightly lower) activity of the segment. Replacement of valine with leucine had only a small deleterious affect, suggesting, as noted above, that extra carbon atoms in the side chains at positions 8 and 9 do not hinder activity.

A D-reverse (retro-inverso) $TSP1_{678}$ peptide retained micromolar inhibitory activity, suggesting that the natural peptide

Table 3. Activities of TSP1 Peptide Derivatives for Inhibiting α3β1-Dependent Adhesion of MDA-MB-435 Breast Carcinoma Cells

peptide	sequence	features	IC_{50} (μM)
678	FQGVLQNVRFVF	native TSP1 sequence	3.5[a]
702	FQGVLQNVKFVF	R → K	6[a]
694	FQGVLQNVHFVF	R → H	54[a]
703	FQGVLQNVQFVF	R → Q	>100[a]
686	FQGVLQAVRFVF	N → A	~300
717	FQGVLQQVRFVF	N → Q	27
718	FQGVLQDVRFVF	N → D	13
719	FQGVLQNLRFVF	V → L	17
709	acetyl-all D-FVFRVNQLVGQF-amide	D-reverse TSP1 sequence	16
730	CNVRC	cyclic form of TSP1 motif	>300
731	CNGRC	cyclic analogue of α5β1 integrin antagonist[34]	>300

[a] Data from ref 13.

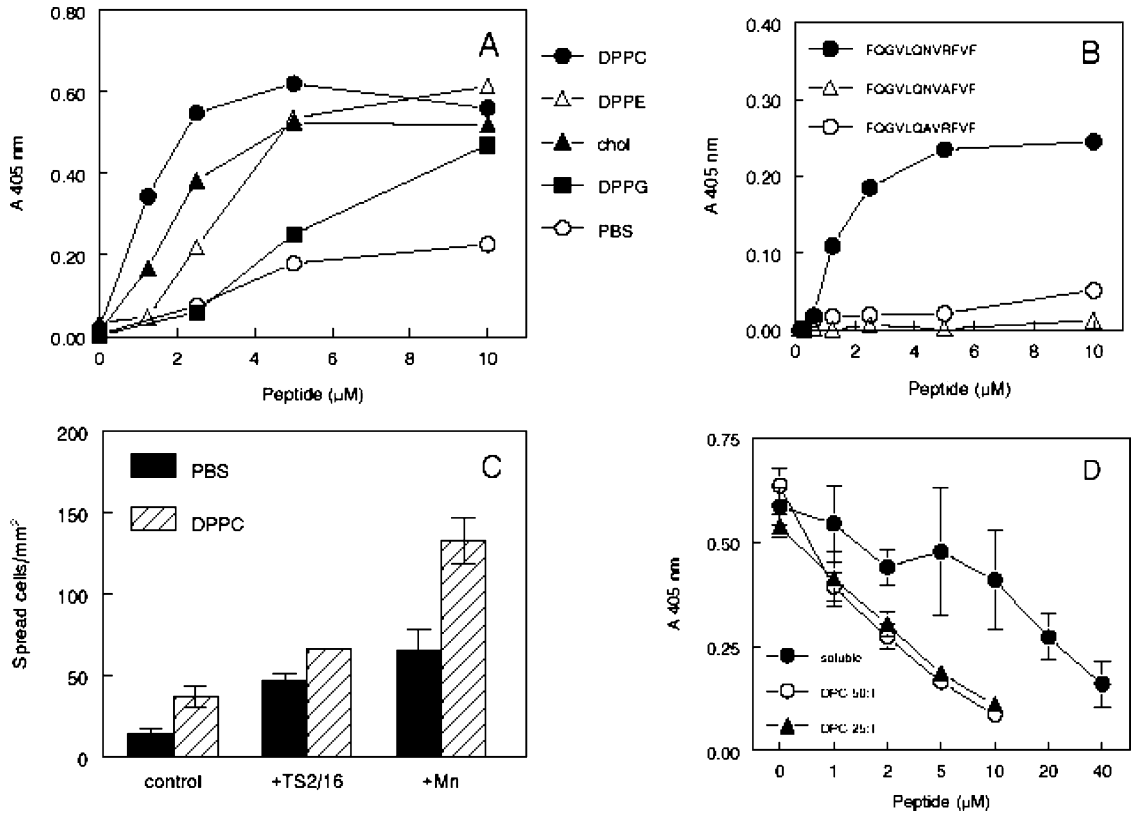

Figure 3. (A). The adhesive activity of $TSP1_{678}$ is enhanced in phospholipid monolayers. Peptides were adsorbed on polystyrene microtiter plate wells by partitioning from PBS or onto monolayers of DPPC, PE, PG, or cholesterol from 1:1 methanol:water. Adhesion of MDA-MB-435 breast carcinoma cells was determined by detection of cell-associated hexosaminidase. Released *p*-nitrophenolate was detected by absorbance at 405 nm and is presented at the mean of triplicate determinations. (B) The NVR motif is required for activity of peptide in a DPPC monolayer. $TSP1_{678}$, $TSP1_{686}$, or $TSP1_{690}$ were immobilized in DPPC monolayers, and MDA-MB-435 cell adhesion was quantified as in panel A. (C) Cell adhesion on peptide in a DPPC monolayer is enhanced by β1 integrin activation. Cell adhesion to wells coated with 2.5 μM $TSP1_{678}$ directly or in a DPPC monolayer was determined without additions or in the presence of 5 μg/mL of the β1 activating antibody TS2/16 or 0.2 mM Mn^{2+}. (D). Incorporation of peptide in DPC micelles enhances its ability to inhibit cell adhesion. Cell adhesion to wells coated with 5 μM $TSP1_{678}$ was determined in the presence of the indicated concentrations of soluble $TSP1_{678}$ or $TSP1_{678}$ incorporated into DPC micelles at molar ratios of 1:25 or 1:50.

backbone is unnecessary and that presenting the biologically relevant side chains on a nonpeptidyl scaffold could yield active compounds. Cyclic peptides often display increased integrin inhibitory activities. However, the functional groups were evidently restricted to undesirable orientations in the cyclic analogue (cyclo)CNVRC, since this analogue was inactive. Similarly, the cyclic analogue (cyclo)CNGRC was inactive, although the same peptide is an active α5β1 integrin antagonist.[34]

Immobilization in Phosphatidylcholine Enhances the α3β1 Integrin Binding Activity of $TSP1_{678}$. To better replicate the predicted environment of the peptide in intact TSP1, $TSP1_{678}$ was immobilized in monolayers of several lipids and tested for adhesive activity using an α3β1-dependent breast cancer cell line (Figure 3A). As indicated by a left shift of the dose−response curve, immobilization in lipid monolayers enhanced the dose-dependent adhesive activity of $TSP1_{678}$ relative to the same peptide adsorbed directly on plastic in the order dipalmitoyl phosphatidylcholine (DPPC) > cholesterol > dipalmitoyl phosphatidylethanolamine > dipalmitoyl phosphatidylglycerol. Because DPPC showed the best activity, this lipid was used for subsequent studies, although similarly enhanced activity was observed using dimyristoyl phosphatidylcholine (results not shown). Adhesive activity of the peptide in a DPPC monolayer retained the requirement for the essential NVR motif, in that $TSP1_{686}$ had minimal adhesive activity and $TSP1_{690}$ was inactive in DPPC monolayers (Figure 3B). Adhesion to $TSP1_{678}$ immobilized in DPPC was also confirmed to be β1 integrin

Table 4. ^{1}H Chemical Shifts of $TSP1_{678}$ in DPC Micelles

	chemical shift (ppm)			
residue	NH	$C^\alpha H$	$C^\beta H$	others
Phe^1	n.d.[a]	4.25	3.16; 3.12	$\delta H_{2,6}$ 7.20;[b]
Gln^2	8.90	4.33	2.03; 1.89	γCH_2 2.27; δNH_2 7.51; 6.80
Gly^3	8.04	3.99; 3.85	-	-
Val^4	8.55	3.98	2.09	γCH_3 0.96; 0.90
Leu^5	8.54	4.09	1.72; 1.52	γH 1.55; δCH_3 0.92; 0.84
Gln^6	8.17	4.00	1.98	γCH_2 2.29; δNH_2 7.51; 6.82
Asn^7	8.05	4.66	2.79; 2.74	δNH_2 7.59; 7.02
Val^8	7.78	3.93	2.15	γCH_3 0.96; 0.87
Arg^9	7.97	4.14	1.66	γCH_2 1.40; δCH_2 3.04; ϵNH 7.35
Phe^{10}	7.80	4.49	3.11; 2.96	$\delta H_{2,6}$ 7.21; $\epsilon H_{3,5}$ 7.24;[b]
Val^{11}	7.48	3.95	1.91	γCH_3 0.74; 0.66
Phe^{12}	7.57	4.48	3.14; 2.87	$\delta H_{2,6}$ 7.20; $\epsilon H_{3,5}$ 7.13;[b]

[a] Not detectable, most likely exchange broadened. [b] Missing aromatic proton chemical shifts were not resolved and could not be unambiguously identified.

dependent by enhancement of adhesion in the presence of the β1 activating antibody TS2/16 and by Mn^{2+} (Figure 3C).

$TSP1_{678}$ exhibits Enhanced Activity in DPC Micelles. To establish activity of the peptide under conditions that could be applied to NMR studies, $TSP1_{678}$ was incorporated into DPC micelles at different molar ratios, and these lipid−peptide aggregates were tested as competitive inhibitors of cell adhesion to immobilized $TSP1_{678}$ peptide (Figure 3D). On the basis of the dose dependence, micellar $TSP1_{678}$ was approximately 8-fold more active on a molar basis than the soluble peptide. This enhancement presumably results from both conformational stabilization and the potential for multivalent binding of the micelle-bound peptide to cell surface α3β1 integrin. DPC micelles alone did not inhibit adhesion at the concentrations used in this experiment (results not shown). These results establish that $TSP1_{678}$ retains integrin binding activity when associated with DPC micelles.

Description of the Structure of $TSP1_{678}$ in DPC Micelles. $TSP1_{678}$ is situated in a β-sheet structure of TSPN-1,[13,16] wherein one face of the strand comprising $TSP1_{678}$ is partially exposed to solvent and the other points toward the hydrophobic core of the protein. We therefore were highly interested to also study the structure of $TSP1_{678}$ in a micellar environment. Although the solubility of $TSP1_{678}$ in DPC-micelles was found to be higher than in water, aggregation of the peptide at a concentration of ~2 mM $TSP1_{678}$ in 200 mM DPC was evident due to the high viscosity of the otherwise clear solution. In accordance with this hypothesis, NMR-spectra showed at least three strongly broadened sets of resonances. The viscosity problem was resolved by diluting the samples to approximately 0.3 mM $TSP1_{678}$ dissolved in 210 mM DPC ($H_2O/^2H_2O$ 9:1). At this lowered concentration, NMR spectra were of much higher quality but analysis was still hampered by the broadened lines due to the increased reorientation times of the peptide in complex with the micelles (line widths at half-height of ~20 Hz, on average, at 300 K). This was particularly evident in the TOCSY-spectra which showed very low signal-to-noise-ratios and viable data could only be obtained by using the relaxation optimized MOCCA-XY16 multiple pulse sequence.[31] A sufficient quality NOESY spectrum (80 ms mixing time) used to derive structural restraints required long acquisition times at high field (900 MHz) with cryogenic probe technology. Notwithstanding, nearly complete resonance assignments for the individual spin systems were obtained using both the TOCSY and NOESY data. These assignments are listed in Table 4.

The uniform measured line width of approximately 20 Hz and the absence of positive NOE-connectivities in the NOESY

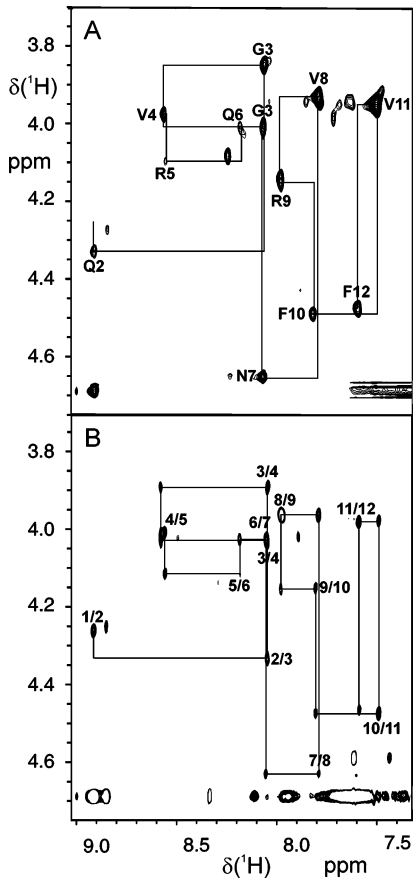

Figure 4. The H_N-H_α region of the 70 ms MOCCA-XY16 TOCSY (A) and the 80 ms NOESY spectrum (B) of $TSP1_{678}$ dissolved in 210 mM [^{2}H]DPC and $^1H_2O/\ ^2H_2O$ (9:1). A complete sequential walk through the assignments is shown in both spectra with intraresidual H_N-H_α cross-peaks marked with single letter code and amino acid number in the TOCSY and interresidual cross-peaks labeled accordingly in the NOESY spectrum.

spectrum clearly indicated that the peptide was associated with the DPC micelles and that it was this bound structure that was analyzed in these samples. An expansion of the NH−Hα region from both TOCSY and NOESY spectra obtained for the $TSP1_{678}$ peptide in micelles is presented in Figure 4 showing the sequential walk through the peptide backbone. Difficulties in the assignment process were due to amide resonance chemical shift degeneracy for Val8 and Phe10 (7.79 ppm), Gly3 and Asn7 (8.04 ppm), and Val4 and Leu5 (8.54 ppm), respectively. However, adequate dispersion of the side chain connectivities permitted unambiguous assignment of all amino acids. Close inspection of the chemical shifts of the peptide in DPC micelles showed that, as was also evident for the sample in water, residues Gln6 to Phe12 were shifted upfield relative to the random coil H_N and H_α values, indicating a possible helical structural arrangement for the C-terminal half of the peptide. The upfield shift is more pronounced than for $TSP1_{678}$ in water and together with the large range of amide chemical shifts for this region further supported a more defined structure for residues Gln6-Phe12. Significant downfield shifts for the amide resonances were observed for residues Gln2, Val4, and Leu5, for which, however, no medium or long-range NOE-connectivities could be found to support a defined structure. It should be noted that residues Leu5 and Gln6 show amide signals with significantly reduced intensities. The most obvious interpretation for this is a relatively slow motion in the microsecond to millisecond time range at the central residues.

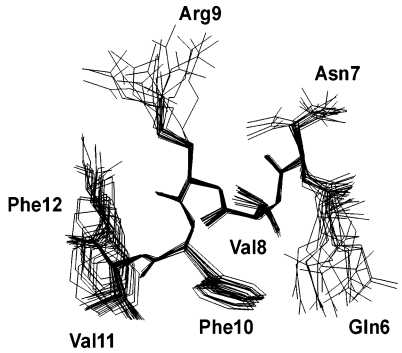

Figure 5. Overlay of 20 best structures of the C-terminal half (Gln6-Phe12) of $TSP1_{678}$ in DPC-micelles. Only residues 7−11 are superimposed. All heavy atoms are displayed.

The broad line widths of the resonances did not allow the measurement of scalar coupling constants, and as a result no dihedral angle constraints could be used in the structure calculations. However, numerous medium-range cross-peaks in the Hα−HN, Hβ−HN and side chain-HN regions for the C-terminal segment (Gln6-Phe12) of $TSP1_{678}$ were observed; in particular, NOESY cross-peaks between the side chains of Val8 and Val11 with the phenyl protons of Phe10 and Phe12, respectively, resulted in a highly defined structure in this part of the molecule (Figure 5 and Table 5). Furthermore, the complete absence of NOEs to the side chain protons of Arg9 indicate that this residue is located on the opposite side to the hydrophobic face made up by Val8, Phe10, Val11, and Phe12 (depicted in Figure 5). The absence of medium and long range NOE connectivities for residues Phe1 to Leu5 leads to a largely undefined, extended structure for the N-terminal segment of $TSP1_{678}$. A comparison of the XPLOR-derived structures of $TSP1_{678}$ in water and DPC micelles is shown in Figure 6. To highlight the convergence of the fit for the critical integrin-binding residues, only the NVR motif is overlayed in each depiction. It is readily apparent that this segment is defined in both water (Figure 6A) and DPC micelles (Figure 6B). It is also clear that there is a great deal of scatter in the N-terminal residues for both systems, but the C-terminal seven residues maintain a distinct conformational preference in the micelle solution (Figure 6B). An additional perspective for the putative binding face of $TSP1_{678}$ is shown in Figure 7A, where the electrostatic surface of the lowest energy structure for the peptide in DPC micelles, calculated with the program GRASP, is shown. A well defined binding pocket of the most important residues Asn7, Val8, and Arg9 is clearly evident. In the lowest energy structure, Phe1, Gly3, Val4, and Phe12, residues that have also been shown to be important for integrin binding,[13] are placed very close to the main binding site, while all other, less important residues point away from the potential binding pocket. The N-terminal part of the structure, however, is not well defined, and the positions of Phe1, Gly3, and Val4 in Figures 5 and 7A must be considered flexible. On the other hand, the position of Phe12 at the C-terminus is well defined, and the motif spanned by Val8-Phe12 may serve to initiate the turn leading to the α6 helix in the full TSPN-1 protein.[16]

Discussion

It has been securely established that aberrant expression of the α3β1 integrin plays an integral role in the invasiveness of many different tumor types.[35] Consequently, the design of α3β1 integrin binding antagonists has emerged as an intriguing area in antimetastatic drug discovery. In this report, we have determined the solution conformation in both water and lipid micelles of a 12-residue peptide segment ($TSP1_{678}$) of TSP1 that was previously shown to bind to α3β1 integrin.[13] Interactions of $TSP1_{678}$ and the TSP1 domain containing this segment with α3β1 modulate tumor and endothelial cell chemotaxis and proliferation in vitro and have antiangiogenic activities in vivo.[14,15,36] These properties suggest that α3β1 integrin interactions with this sequence in TSP1 are critical regulators of tumor progression and metastasis. Since the atomic structure of TSPN-1 is now known, definition of the solution conformation of this functional sequence in different milieus will facilitate both the design and implementation of small molecule antagonists of α3β1 integrin.

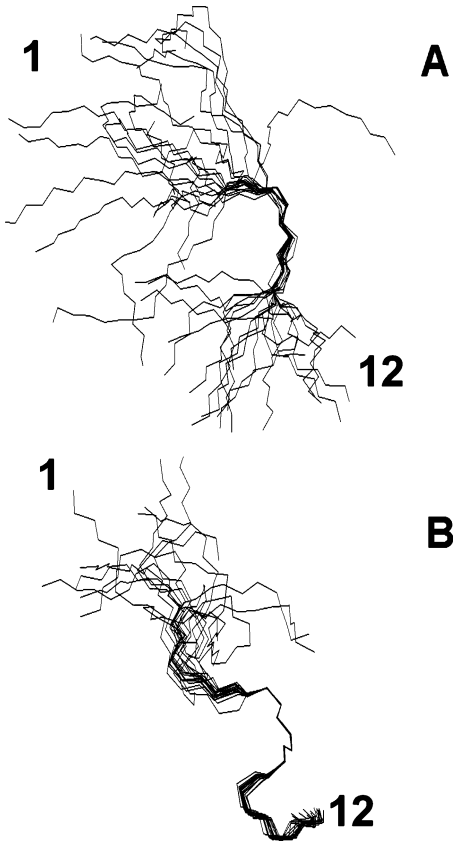

Figure 6. Comparison of the superposition (backbone atoms only) of the 20 lowest energy structures calculated using XPLOR for TSP_{678} in (A) water and (B) DPC micelles. Only residues Asn7-Arg9 are superimposed, and the direction of the backbone is indicated by the N-terminal (1) and C-terminal residues (12).

The conformation of $TSP1_{678}$ in solution was studied by circular dichroism and compared to peptides of identical length where single amino acid substitutions either reduced or abrogated their activity. In all cases, active peptides showed distinct CD signatures that were absent in the inactive analogues. As shown in Figure 1, $TSP1_{678}$ showed the double minimum followed by a large maximum that is characteristic of helical motifs in many proteins.[37] The ellipticities for the negative peaks are about 30% of an entirely α-helical structure. This is most likely due to a mixture of conformations in solution, where propensities for β-structures or turns are also possible. This is illustrated in the NMR data, where no one form dominates in water (Figure 1). Even though it is difficult to speculate on precisely what secondary structural elements the CD spectra define, the data illustrate clearly that active peptides retain some structural integrity in water.

A critical examination of the NMR data in water corroborates some of the features of the CD spectra. As is typically the case

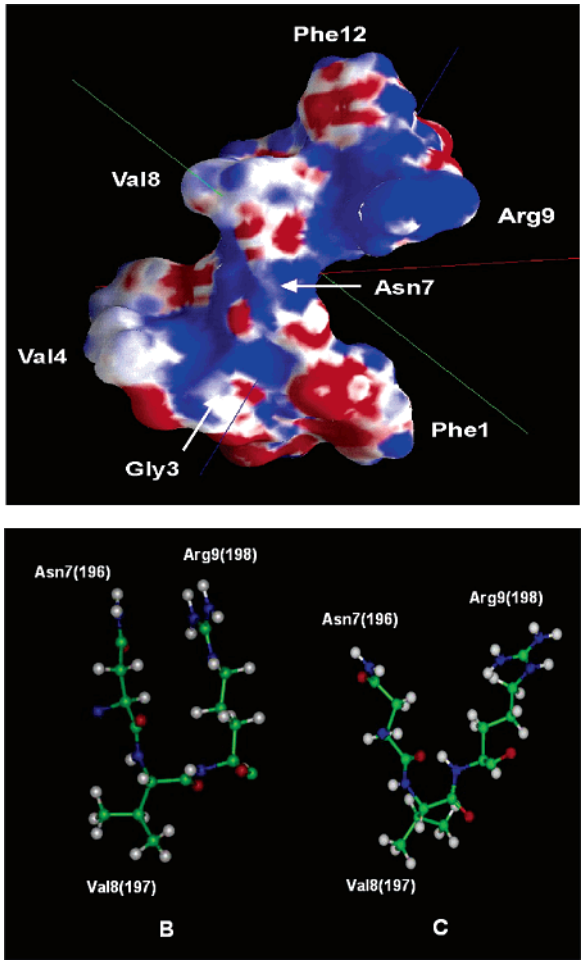

Figure 7. (A) GRASP electrostatic surface of the lowest energy structure of $TSP1_{678}$ in DPC micelles. Negatively charged atoms are colored in red, positive charges are blue. A putative binding surface around residues Asn7, Val8, Arg9, and Phe12 is shown. (B, C) Comparison of the NVR motif from the (B) crystal of the TSPN-1 domain (ref 16) and (C) NMR structure in DPC micelles. The residue side chains are labeled with numbering from the 12-mer peptide. Numbers in parentheses refers to the labeling of the corresponding residues in the intact N-terminal domain of the protein.

for small (<25 residues) peptides in aqueous media, $TSP1_{678}$ is primarily unstructured in water. However, some features of the spectra indicate that distinct and stable conformers are also populated in aqueous media. Specifically, the chemical shifts of residues Gln6 − Phe12 resonate upfield of random coil values suggesting a propensity for coil−helix transitions occurring in this portion of the peptide. This behavior may account for the CD spectral signatures that are highly suggestive of significant helical content for the peptide in water. In addition, NMR analysis showed that the residues known to be critical for integrin binding seem to be structurally ordered in both water and DPC micelles. Although virtually no long-range restraints were derived from the NOE data, modeling the peptide with XPLOR revealed a convergence of conformations, in which the critical NVR motif was reasonably well-defined in a bend or loop structure.

Further evaluation of the structure was performed in a membrane-mimicking environment. Two factors guided us to immobilize $TSP1_{678}$ in lipid bilayers to further study the integrin binding and three-dimensional conformation of the peptide. The TSPN-1 domain from which TSP_{678} is derived is evolutionarily related to the pentraxin family and the G modules of laminins.[13,17,38] On the basis of atomic structures of pentraxins[39] and the laminin α2 G3-G4 modules,[38] the $TSP1_{678}$ sequence in TSP1 was predicted to reside in a β-sheet sandwich fold, wherein many of the nonpolar side chains of this peptide would interact with nonpolar side chains contributed by the opposing β-sheet. Therefore, micelles were expected to provide an amphipathic interface that replicates this aspect of the predicted environment of TSP_{678} in native TSP1. The recent crystal structure of TSPN-1 shows that this prediction was accurate, and our assumptions were validated. Second, the limited water solubility of $TSP1_{678}$ could be enhanced in an amphipathic environment. These hypotheses were borne out when the peptide was studied in the presence of various phospholipids. Thus, the adhesive activity of $TSP1_{678}$ was enhanced by immobilizing in phospholipid monolayers, and micellar $TSP1_{678}$ showed enhanced inhibition of α3β1-dependent cell adhesion. Appropriate controls suggested that the binding and inhibitory activities of $TSP1_{678}$ were not due to the lipid but stemmed from the altered environment of the peptide. Presumably, immobilization of this highly flexible peptide on lipid monolayers effectively stabilizes a specific conformation compatible with integrin recognition.

NMR studies of $TSP1_{678}$ in DPC micelles revealed that a major readjustment of the structure occurred when presented in a micellar milieu. Medium-range NOEs appeared when $TSP1_{678}$ was dissolved in DPC micelles. The majority of these new restraints were evident in the C-terminal half of the peptide, and as a result, structure calculations converged to a well-ordered and stable fold for this segment of the peptide. As was shown for $TSP1_{678}$ in water, the first five residues remained primarily unstructured. However, specific side chains from residues Phe1, Gly3, and Val4 may also be components that help define the electronic character of the binding surface of the most stable fold. The GRASP surface in Figure 7A shows the charge distribution on the surface of what may be considered the "binding" face of the peptide. This putative binding surface concentrates both the positive charge and lipophilic character of this half of $TSP1_{678}$. This is most likely due to interactions with the lipid headgroup and tail in the micelle. But most interestingly, all residues that were previously found to be crucial for the inhibition activity of $TSP1_{678}$ (Asn7 and Arg9 as well as Phe1, Phe12, and Val4) are located on the same face of the molecule. When the structure of the NVR motif in lipid is compared to conformation of the same residues from the protein crystal structure (Figures 7B and 7C), one observes a fork-like disposition of the side chains: The asparagine carboxamide and arginine guanidinium groups are the "prongs" that are exposed on the protein surface while the valine isopropyl group is the "handle" that points toward the protein's hydrophobic core. These results validate a model where this peptide may assume a similar polar/nonpolar directionality in the lipid media.

The structure for the α3β1-binding motif we defined in $TSP1_{678}$ shares some characteristics with previously studied integrin binding sites. The most extensively studied integrin binding motif is the RGD sequence in fibronectin, which exists in a loop that protrudes from the surface of the tenth type III repeat. Studies using conformationally restricted peptides have demonstrated that specific orientations of the Arg and Asp side chains are required for specific binding to the two integrins that recognize this sequence, α5β1 and αvβ3. The TSP sequence recognized by α3β1 shares an essential Arg residue with the fibronectin motif, and Asn may serve an equivalent function for α3β1 binding as the Asp does for α5β1. The essential Asp residues in VCAM-1 and invasin are also presented in loops,[40] as are some non-RGD integrin ligands such as the disintegrin obtustatin.[41] Since the overall secondary structure for the

Table 5. Structural Statistics of the 12 Best NOE-Derived Structures of $TSP1_{678}$ in DPC Micelles

total no. of distance constraints	219
no. of intraresidue constraints	128
no. of sequential constraints	72
no. of medium to long-range constraints	19
distance violations	
number > 0.5 Å	0
number > 0.2 Å	10.50 ± 0.75 (9.. 12)
RMS deviations from ideal geometry	
covalent bonds (Å)	0.0070 ± 0.00018 (0.007.. 0.008)
covalent angles (Å)	0.7484 ± 0.0172 (0.691.. 0.79)
improper (degrees)	0.3997 ± 0.0192 (0.365.. 0.45)
NOE	0.0823 ± 0.0011 (0.081.. 0.085)
energies (kcal/mol)	
overall	150.23 ± 2.69 (144.87.. 154.98)
bond	10.53 ± 0.45 (9.74.. 11.38)
angle	31.94 ± 1.38 (27.29.. 35.61)
improper	2.34 ± 0.33 (1.80.. 3.15)
VDW	26.47 ± 2.38 (22.72.. 30.09)
NOE	78.86 ± 1.51 (76.42.. 83.86)
pairwise RMSD (Å)	
residues 7-12	
backbone	0.29
heavy	1.29

TSPN-1 module is primarily β-sheet, the $TSP1_{678}$ sequence may more closely resemble ICAM ligands that interact with I domain-containing integrins, wherein the essential residues are recognized by the integrins in the context of β-strands rather than loops.[42,43]

The TSPN-1 module contains three known integrin binding sites. The binding sequences identified for $\alpha4\beta1$[44] and $\alpha6\beta1$[36] integrins have now been shown[16] to reside in either a loop ($\alpha4\beta1$) or within a strand-loop segment ($\alpha6\beta1$) whereas the $\alpha3\beta1$ integrin binding site in TSPN-1 seems to resemble the β-strand recognition paradigm of the ICAMs.[42] Thus, the enhanced activity of the $\alpha3\beta1$-binding peptide when associated with micelles may result from the manner in which the amino acid side chains are arranged on the lipid surface and how this disposition compares to those residues embedded in the protein fold. The structural data presented here could guide the design of specific $\alpha3\beta1$ antagonists. Our previous studies suggest that $\alpha3\beta1$ antagonists would be useful inhibitors of angiogenesis. $TSP1_{678}$ inhibited proliferation of human umbilical vein and microvascular endothelial cells in vitro and inhibited endothelial cell migration in a scratch wound healing model.[15] The antiproliferative activity of this peptide may result from its inhibiting ligand-induced signals from $\alpha3\beta1$ integrin that cooperate with growth factors to activate MAP kinase signaling in endothelial cells.[45] In the chick chorioallantoic membrane (CAM) angiogenesis assay, $TSP1_{678}$ inhibited angiogenic responses stimulated by VEGF or FGF2 alone and by a combination of the two growth factors.[15] Thus, $\alpha3\beta1$ antagonists may inhibit angiogenesis stimulated by a variety of agonists. Because $TSP1_{678}$ acted specifically on endothelial cells lacking mature cell−cell contacts, $\alpha3\beta1$ antagonists may show selectivity for the leaky vasculature characteristic of tumors.

$\alpha3\beta1$ antagonists may also have direct effects on tumor cells that would be therapeutically useful. Small cell lung carcinoma (SCLC) cells express $\alpha3\beta1$ and use it as a TSP1 receptor.[14] $TSP1_{678}$ mediated SCLC cell adhesion and outgrowth of neurite-like processes from the cells. SCLC proliferation was also inhibited by $TSP1_{678}$. The morphological and antiproliferative activities of $TSP1_{678}$ are consistent with induction of neurotypic differentiation. Therefore, $\alpha3\beta1$ antagonists may be useful to decrease the malignant character of SCLC through inducing differentiation of the tumor cells into a form that is less rapidly disseminated and may be more sensitive to chemotherapeutic agents. $\alpha3\beta1$ antagonists could be used to verify these in vitro responses in an animal model of SCLC.

Finally, $\alpha3\beta1$ expression was reported to be significantly increased in breast tumor metastases.[46] Function-blocking anti-$\alpha3\beta1$ antibodies significantly inhibited the adhesion of MDA-MB-231 breast cancer cells to bone matrices.[47] Small molecule antagonists based on $TSP1_{678}$ may have similar activities to inhibit breast cancer metastasis. In addition, a recent report found that cyclic peptides ligands of $\alpha3\beta1$ conjugated to fluorophores could target and image several ovarian adenocarcinoma cell lines.[48] Results such as this add further validity to the importance of defining an $\alpha3\beta1$ pharmacophore model.

On the basis of the intriguing biological data outlined above, the limited SAR outlined in Table 2 combined with the $TSP1_{678}$ structure could provide a starting point for rational design of nonpeptide antagonists specific for the $\alpha3\beta1$ integrin. Similar approaches have been used previously to design and synthesize potent and specific antagonists for the platelet integrin $\alpha_{IIb}\beta_3$,[49] $\alpha v\beta3$,[50] and $\alpha4\beta1$.[51] A program using validated concepts for peptidomimetic design would be a worthwhile endeavor for constructing novel antiadhesive and antiangiogenic agents.

From the work described here and the recent crystal of TSPN-1, the design of a peptidomimetic of $TSP1_{678}$ may require a scaffold where the critical side chain functional groups reside on appropriate sides of a narrow template. Simple cyclization strategies that may not be appropriate (Table 3) since the distinct directionality of each side chain may need tighter conformational restriction. The construction of carbocyclic[52] or saccharide-type scaffolds[53] with defined stereochemical branch points for each residue may provide a rational starting point. Relevant examples of this concept were reported by the Kessler group who synthesized both $\alpha4\beta1$[54] and $\alpha4\beta7$[55] integrin antagonists on simple carbohydrate templates. In addition, the lack of structure in the N-terminal half of $TSP1_{678}$ may allow the complete replacement of this segment of the molecule without sacrificing potency. Work in this area is currently in progress.

Acknowledgment. J.F. and B.L. thank the Fonds der Chemischen Industrie and the Deutsche Forschungsgemeinschaft (Emmy Noether fellowship LU-835/1-3) for financial support. We also thank O. Hiltner and W. Günther for technical assistance. J.J.B. and D.D.R. were supported by the Intramural Research Program of the National Cancer Institute.

References

(1) Hynes, R. O. Integrins: bidirectional, allosteric signaling machines. *Cell* **2002**, *110*, 673−687.
(2) Hood, J. D.; Cheresh, D. A. Role of integrins in cell invasion and migration. *Nat. Rev. Cancer* **2002**, *2*, 91−100.
(3) Arnaout, M. A.; Goodman, S. L.; Xiong, J. P.; Stehle, T.; Zhang, R.; Joachimiak, A.; Frech, M. Coming to grips with integrin binding to ligands. *Curr. Opin. Cell Biol.* **2002**, *14*, 641−651.
(4) Xiong, J. P.; Stehle, T.; Zhang, R.; Joachimiak, A.; Frech, M.; Goodman, S. L.; Arnaout, M. A. Crystal structure of the extracellular segment of integrin alpha Vbeta3 in complex with an Arg-Gly-Asp ligand. *Science* **2002**, *296*, 151−155.
(5) Springer, T. A. Predicted and experimental structures of integrins and beta-propellers. *Curr. Opin. Struct. Biol*. **2002**, *12*, 802−813.
(6) Pierschbacher, M. D.; Ruoslahti, E. Cell attachment activity of fibronectin can be duplicated by small synthetic fragments of the molecule. *Nature* **1984**, *309*, 30−33.
(7) Main, A. L.; Harvey, T. S.; Baron, M.; Boyd, J.; Campbell, I. D. The three-dimensional structure of the tenth type III module of fibronectin: an insight into RGD-mediated interactions. *Cell* **1992**, *71*, 671−678.
(8) Pierschbacher, M. D.; Ruoslahti, E. Influence of stereochemistry of the sequence Arg-Gly-Asp-Xaa on binding specificity in cell adhesion. *J. Biol. Chem.* **1987**, *262*, 17294−17298.
(9) Emsley, J.; Knight, C. G.; Farndale, R. W.; Barnes, M. J.; Liddington, R. C. Structural basis of collagen recognition by integrin alpha2beta1. *Cell* **2000**, *101*, 47−56.

(10) Ruoslahti, E. RGD and other recognition sequences for integrins. *Ann. Rev. Cell Dev. Biol.* **1996**, *12*, 697−715.
(11) Loftus, J. C.; Liddington, R. C. New insights into integrin-ligand interaction. *J. Clin. Invest.* **1997**, *100*, 77−81.
(12) Gehlsen, K. R.; Sriramarao, P.; Furcht, L. T.; Skubitz, A. P. A synthetic peptide derived from the carboxy terminus of the laminin A chain represents a binding site for the alpha 3 beta 1 integrin. *J. Cell Biol.* **1992**, *117*, 449−459.
(13) Krutzsch, H. C.; Choe, B.; Sipes, J. M.; Guo, N.; Roberts, D. D. Identification of an α3β1 integrin recognition sequence in thrombospondin-1. *J. Biol. Chem.* **1999**, *274*, 24080−24086.
(14) Guo, N.; Templeton, N. S.; Al-Barazi, H.; Cashel, J. A.; Sipes, J. M.; Krutzsch, H. C.; Roberts, D. D. Thrombospondin-1 promotes α3β1 integrin-mediated adhesion and neurite-like outgrowth and inhibits proliferation of small cell lung carcinoma cells. *Cancer Res.* **2000**, *60*, 457−466.
(15) Chandrasekaran, L.; He, C.-Z.; Al-Barazi, H. O.; Krutzsch, H. C.; Iruela-Arispe, M. L.; Roberts, D. D. Cell contact-dependent activation of α3β1 integrin modulates endothelial cell responses to thrombospondin-1. *Mol. Biol. Cell* **2000**, *11*, 2885−2900.
(16) Tan, K.; Duquette, M.; Liu, J. H.; Zhang, R. G.; Joachimiak, A.; Wang, J. H.; Lawler, J. The structures of the thrombospondin-1 N-terminal domain and its complex with a synthetic pentameric heparin. *Structure* **2006**, *14*, 33−42.
(17) Beckmann, G.; Hanke, J.; Bork, P.; Reich, J. G. Merging extracellular domains: fold prediction for laminin G-like and amino-terminal thrombospondin-like modules based on homology to pentraxins. *J. Mol. Biol.* **1998**, *275*, 725−730.
(18) Hohenester, E.; Tisi, D.; Talts, J. F.; Timpl, R. The crystal structure of a laminin G-like module reveals the molecular basis of alpha-dystroglycan binding to laminins, perlecan, and agrin. *Mol. Cell* **1999**, *4*, 783−792.
(19) Marion, D.; Ikura, M.; Tschudin, R.; Bax, A. Rapid Recording of 2D NMR Spectra without Phase Cycling. Application to the Study of Hydrogen Exchange in Proteins. *J. Magn. Reson.* **1989**, *85*, 393−399.
(20) Palmer, A. G.; Cavanagh, J.; Wright, P. E.; Rance, M. Sensitivity Improvement in Proton-Detected 2-Dimensional Heteronuclear Correlation Nmr-Spectroscopy. *J. Magn. Reson.* **1991**, *93*, 151−170.
(21) Cavanagh, J.; Palmer, A. G.; Wright, P. E.; Rance, M. Sensitivity Improvement in Proton-Detected 2-Dimensional Heteronuclear Relay Spectroscopy. *J. Magn. Reson.* **1991**, *91*, 429−436.
(22) Liu, M. L.; Mao, X. A.; Ye, C. H.; Huang, H.; Nicholson, J. K.; Lindon, J. C. Improved WATERGATE pulse sequences for solvent suppression in NMR spectroscopy. *J. Magn. Reson.* **1998**, *132*, 125−129.
(23) Hwang, T. L.; Shaka, A. J. Multiple-pulse mixing sequences that selectively enhance chemical exchange or cross-relaxation peaks in high-resolution NMR spectra. *J. Magn. Reson.* **1998**, *135*, 280−287.
(24) Kneller, D. G.; Kuntz, I. D. Ucsf Sparky − an NMR Display, Annotation and Assignment Tool. *J. Cell. Biochem.* **1993**, 254.
(25) Braunschweiler, L.; Ernst, R. R. Coherence Transfer by Isotropic Mixing: Application to Proton Correlation Spectroscopy. *J. Magn. Reson.* **1983**, *53*, 521−528.
(26) Bax, A.; Davis, D. G. MLEV-17-based 2D homonuclear magnetization transfer spectroscopy. *J. Magn. Reson.* **1985**, *65*, 355−360.
(27) Shaka, A. J.; Lee, C. J.; Pines, A. Iterative Schemes for Bilinear Operators; Application to Spin Decoupling. *J. Magn. Reson.* **1988**, *77*, 274−293.
(28) Bothner-By, A. A.; Stevens, R. L.; Lee, J.; Warren, C. D.; Jeanloz, R. W. Structure Determination of a Tetrasaccharide: Transient Nuclear Overhauser Effects in the Rotating Frame. *J. Am. Chem. Soc.* **1984**, *106*, 811−813.
(29) Bax, A.; Davis, D. G. Practical Aspects of Two-Dimensional Transverse NOE Spectroscopy. *J. Magn. Reson.* **1985**, *63*, 207−213.
(30) Wishart, D. S.; Bigam, C. G.; Yao, J.; Abildgaard, F.; Dyson, H. J.; Oldfield, E.; Markley, J. L.; Sykes, B. D. H-1, C-13 and N-15 Chemical-Shift Referencing in Biomolecular Nmr. *J. Biomol. NMR* **1995**, *6*, 135−140.
(31) Furrer, J.; Kramer, F.; Marino, J. P.; Glaser, S. J.; Luy, B. Homonuclear Hartmann−Hahn transfer with reduced relaxation losses by use of the MOCCA-XY16 multiple pulse sequence. *J. Magn. Reson.* **2004**, *166*, 39−46.
(32) Nilges, M.; Gronenborn, A. M.; Brunger, A. T.; Clore, G. M. Determination of 3-Dimensional Structures of Proteins by Simulated Annealing with Interproton Distance Restraints − Application to Crambin, Potato Carboxypeptidase Inhibitor and Barley Serine Proteinase Inhibitor-2. *Protein Eng.* **1988**, *2*, 27−38.
(33) Wilson, K. E.; Li, Z.; Kara, M.; Gardner, K. L.; Roberts, D. D. β1 integrin- and proteoglycan-mediated stimulation of T lymphoma cell adhesion and mitogen-activated protein kinase signaling by thrombospondin-1 and thrombospondin-1 peptides. *J. Immunol.* **1999**, *163*, 3621−3628.
(34) Koivunen, E.; Wang, B. C.; Ruoslahti, E. Isolation of A Highly Specific Ligand for the Alpha(5)Beta(1) Integrin from A Phage Display Library. *J. Cell Biol.* **1994**, *124*, 373−380.
(35) Katabami, K.; Kato, T.; Sano, R.; Ogura, M.; Mizuno, H.; Itoh, S.; Tsuji, T. Characterization of the promoter for the alpha 3 integrin gene in various tumor cell lines: Roles of the Ets- and Sp-family of transcription factors. *J. Cell. Biochem.* **2006**, *97*, 530−543.
(36) Calzada, M. J.; Sipes, J. M.; Krutzsch, H. C.; Yurchenco, P. D.; Annis, D. S.; Mosher, D. F.; Roberts, D. D. Recognition of the N-terminal modules of thrombospondin-1 and thrombospondin-2 by alpha6beta1 integrin. *J. Biol. Chem.* **2003**, *278*, 40679−40687.
(37) Woody; R. W. Theory of Circular Dichroism in Proteins. In *Circular Dichroism and the Conformational Analysis of Biomolecules*; Gerald D Fasman Ed.; Plenum Press: New York, 1996; pp 25−67.
(38) Timpl, R.; Tisi, D.; Talts, J. F.; Andac, Z.; Sasaki, T.; Hohenester, E. Structure and function of laminin LG modules. *Matrix Biol.* **2000**, *19*, 309−317.
(39) Srinivasan, N.; White, H. E.; Emsley, J.; Wood, S. P.; Pepys, M. B.; Blundell, T. L. Comparative analyses of pentraxins: implications for protomer assembly and ligand binding. *Structure* **1994**, *2*, 1017−1027.
(40) Hamburger, Z. A.; Brown, M. S.; Isberg, R. R.; Bjorkman, P. J. Crystal structure of invasin: a bacterial integrin-binding protein. *Science* **1999**, *286*, 291−295.
(41) Paz Moreno-Murciano, M.; Monleon, D.; Marcinkiewicz, C.; Calvete, J. J.; Celda, B. NMR solution structure of the non-RGD disintegrin obtustatin. *J. Mol. Biol.* **2003**, *329*, 135−145.
(42) Casasnovas, J. M.; Pieroni, C.; Springer, T. A. Lymphocyte function-associated antigen-1 binding residues in intercellular adhesion molecule-2 (ICAM-2) and the integrin binding surface in the ICAM subfamily. *Proc. Natl. Acad. Sci. U. S. A.* **1999**, *96*, 3017−3022.
(43) Wang, J.; Springer, T. A. Structural specializations of immunoglobulin superfamily members for adhesion to integrins and viruses. *Immunol. Rev.* **1998**, *163*, 197−215.
(44) Li, Z.; Calzada, M. J.; Sipes, J. M.; Cashel, J. A.; Krutzsch, H. C.; Annis, D.; Mosher, D. F.; Roberts, D. D. Interactions of thrombospondins with α4β1 integrin and CD47 differentially modulate T cell behavior. *J Cell Biol.* **2002**, *157*, 509−519.
(45) Aplin, A. E.; Short, S. M.; Juliano, R. L. Anchorage-dependent regulation of the mitogen-activated protein kinase cascade by growth factors is supported by a variety of integrin alpha chains. *J. Biol. Chem.* **1999**, *274*, 31223−31228.
(46) Morini, M.; Mottolese, M.; Ferrari, N.; Ghiorzo, F.; Buglioni, S.; Mortarini, R.; Noonan, D. M.; Natali, P. G.; Albini, A. The alpha 3 beta 1 integrin is associated with mammary carcinoma cell metastasis, invasion, and gelatinase B (MMP-9) activity. *Int. J. Cancer* **2000**, *87*, 336−342.
(47) van der Pluijm, G.; Vloedgraven, H.; Papapoulos, S.; Lowick, C.; Grzesik, W.; Kerr, J.; Robey, P. G. Attachment characteristics and involvement of integrins in adhesion of breast cancer cell lines to extracellular bone matrix components. *Lab Invest.* **1997**, *77*, 665−675.
(48) Aina, O.; Marik, J.; Gandour-Edwards, R.; Lam, K. Near-infrared optical imaging of ovarian cancer xenografts with novel alpha 3-integrin binding peptide "OA02". *Mol. Imaging* **2005**, *4*, 439−447.
(49) O'Shea, J. C.; Tcheng, J. E. Eptifibatide: a potent inhibitor of the platelet receptor integrin glycoprotein IIb/IIIa. *Expert Opin. Pharmacother.* **2002**, *3*, 1199−1210.
(50) Miller, W. H.; Keenan, R. M.; Willette, R. N.; Lark, M. W. Identification and in vivo efficacy of small-molecule antagonists of integrin alphavbeta3 (the vitronectin receptor). *Drug Discovery Today* **2000**, *5*, 397−408.
(51) Jackson, D. Y. α4 integrin antagonists. *Curr. Pharm. Des.* **2002**, *8*, 1229−1253.
(52) Fischer, P. M. The design, synthesis and application of stereochemical and directional peptide isomers: A critical review. *Current Protein Pept. Sci.* **2003**, *4*, 339−356.
(53) Le, G. T.; Abbenante, G.; Becker, B.; Grathwohl, M.; Halliday, J.; Tometzki, G.; Zuegg, J.; Meutermans, W. Molecular diversity through sugar scaffolds. *Drug Discovery Today* **2003**, *8*, 701−709.
(54) Boer, J.; Gottschling, D.; Schuster, A.; Holzmann, B.; Kessler, H. Design, synthesis, and biological evaluation of alpha(4)beta(1) integrin antagonists based on beta-d-mannose as rigid scaffold. *Angew. Chem.-Int. Ed.* **2001**, *40*, 3870−3873.
(55) Locardi, E.; Boer, J.; Modlinger, A.; Schuster, A.; Holzmann, B.; Kessler, H. Synthesis and structure − Activity relationship of mannose-based peptidomimetics selectively blocking integrin alpha 4 beta 7 binding to mucosal addressin cell adhesion molecule-1. *J. Med. Chem.* **2003**, *46*, 5752−5762.

JM060833L